Article

Applied Spectroscopy
2018, Vol. 72(1) 37–47

DOI: 10.1177/0003702817736516
journals.sagepub.com/home/asp
SAGE

# Variability in the Raman Spectrum of Unpolished Growth and Fracture Surfaces of Pyrite Due to Laser Heating and Crystal Orientation

**Roger N. Bryant[1], Jill D. Pasteris[1,2], and David A. Fike[1,2]**

**Abstract**

Two probable causes of variability in the Raman spectrum of unpolished pyrite are well recognized, in principle, but not always in practice, namely: (1) downshifting of band positions due to laser heating; and (2) variations in the ratios of band intensities due to crystallographic orientation of the sample with respect to the laser's dominant polarization plane. The aims of this paper are to determine whether these variations can be used to acquire additional information about pyrites. Here, using laser Raman microprobe analysis of natural, unpolished pyrite samples, we investigate the magnitude of downshifting of band positions associated with laser heating of different sizes of pyrite grains. We demonstrate that the magnitude of this effect can be large (up to $\sim$10 $cm^{-1}$), negatively proportional to grain size, of greater magnitude than the effect typically attributable to natural intersample differences in trace element (TE) solid solution, and of similar magnitude among bands. Through Raman analysis of naturally occurring faces on pyrite samples at various angles of rotation, we also demonstrate that the three most common faces on pyrite can be distinguished by the ratio of the intensities of the dominant bands. We conclude that for unpolished samples, laser Raman microprobe analysis is most effective as a means of identifying pyrite, and the presence of solid solution therein, when laser power is low enough to avoid substantial heating. Once pyrite has been identified, higher laser powers can be used to produce spectra whose ratios of band intensities indicate the face or crystallographic plane being irradiated.

**Keywords**

Raman spectroscopy, pyrite, laser heating, crystal morphology, crystal size, crystal orientation, trace elements

Date received: 14 March 2017; accepted: 15 September 2017

## Introduction

Mineral identification and further characterization (e.g., size, degree of crystallinity, morphology, and neighboring phases) often provide essential environmental context for interpreting geochemical data. Laser Raman microprobe analysis, in contrast to powder X-ray diffraction (XRD), petrography, and electron microprobe analysis, allows individual grains of 1 μm or less (depending on instrumental configuration) to be assigned an accurate mineral identification. The spectral bands produced by Raman analysis of a mineral are defined by vibrational frequencies indicative of the bonding and symmetry of the mineral structure. The positions of the bands for a mineral can be distinguished from those of other minerals, including polymorphs (e.g., marcasite and pyrite, see Fig. 1).[1] Pyrite is a common accessory phase in many igneous and metamorphic rocks, is often abundant in ore deposits, and also occurs in many sedimentary rocks. Despite the abundance and importance of pyrite, however, its band positions and band intensity ratios in previously published Raman spectra are markedly variable.[1–10] Whether this variability represents analytical artifacts, inconsistent spectral calibration between different instruments and labs, near-surface strain, or real mineral-chemical differences has yet to be addressed. Additionally, if the variability is real, its origin as the result of compositional or morphologic differences remains to be clarified. In this

[1]Department of Earth & Planetary Sciences, Washington University in St. Louis, St. Louis, MO, USA
[2]Institute for Materials Science and Engineering, Washington University in St. Louis, St. Louis, MO, USA

**Corresponding author:**
Roger N. Bryant, Department of Earth & Planetary Sciences, Washington University in St. Louis, 1 Brookings Drive, St. Louis, MO 63130, USA.
Email: rnbryant@wustl.edu

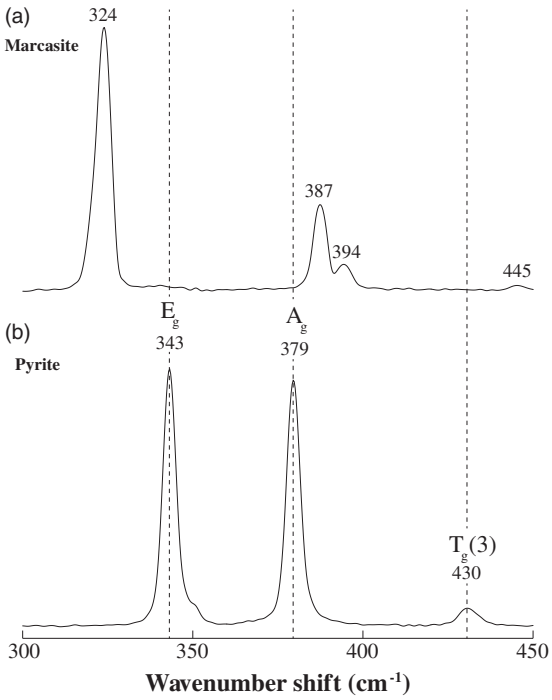


**Figure 1.** Raman spectra of: (a) a 0.3 cm-diameter marcasite sample (Ward's Natural Science) from Vintířov, Bohemia, Czech Republic, and (b) a 1 cm-diameter pyrite sample from Navajún, La Rioja, Spain. All bands are labeled with their positions (calculated as the band midpoint at half maximum intensity). Both spectra were produced using a laser power of 3 mW, an optical objective of 80× and numerical aperture (N.A.) of 0.75, and averaging over 20 spectra each with a collection time of 5 s. The spectral resolution for these spectra is 2.5 cm$^{-1}$.

study, we conduct experiments to evaluate the presence and nature of variability in the Raman spectra of pyrite samples analyzed under controlled conditions. We also explore whether variation in band positions and band intensity ratios can be diagnostic for the presence of chemical impurities and for the morphology of the pyrite crystal.

## Variability in the Raman Spectrum of Pyrite

Crystalline pyrite belongs to the cubic/isometric crystal system, crystal class 2/m$\bar{3}$, with unit cell factor group symmetry of $T_h$. The Raman-active modes are traditionally referred to by their group symmetry properties $E_g$, $A_g$, and $T_g$.[2] We will use that nomenclature here (Fig. 1). Figure 1b shows a typical Raman spectrum of a hand sample of pyrite, with crystals on the order of ~1 cm. The three bands from left to right correspond to the characteristic Raman-active modes for pyrite: the $S_2$ dumb-bell libration ($E_g$); the S–S in-phase, symmetric stretch ($A_g$); and the coupled libration and stretch ($T_g(3)$) modes.[2,4,11] Table I is a compilation of Raman spectral data on pyrite from the literature. Two ways in which the published spectra vary are: (1) the positions (recorded in wavenumbers) of the bands; and (2) the intensity ratios of the bands with respect to each other.

Figure 2 shows the substantial variability in the position of each major band previously published in the literature. A displacement in the position of one band is typically accompanied by sympathetic displacements in the other two bands. The band positions of the $A_g$ and $T_g(3)$ modes of pyrite are positively correlated with the band position of the $E_g$ mode of pyrite, with $R^2$ values of 0.85 and 0.80, respectively.

## Potential Causes of Variability in Band Positions

### *Differential Calibration*

If the Raman instruments in different laboratories are calibrated differently, this could result in apparent offsets in band positions for pyrite samples analyzed in separate labs.[14] Typically, a Si wafer is used as a standard to determine the amount of offset of the measured position from the standard's accepted position due to inaccurate calibration. As all pyrite's bands occur close to that of Si (band at ~520.5 $\Delta$cm$^{-1}$), any amount of offset due to incorrect calibration should be the same for all bands. While calibration error alone may therefore be able to produce the covariance of band positions (with a slope of ~1) seen in Fig. 2, calibration error alone is unlikely to explain the full range of variation in band positions in Table I and Fig. 2.

### *Analytical Artifacts*

Laser heating has been shown to result in downshifting of bands for many materials,[15–28] especially those that are opaque. Pyrite is opaque and has a prominent optical absorption band in the wavelength region of ~300–1200 nm,[29] which encompasses the wavelength of lasers typically used for Raman analysis (e.g., 532 nm, this study), so this effect is expected to be relevant to pyrite. As pyrite's bands occur close together, this effect should be of similar magnitude for each band,[27] potentially facilitating the covariance of band positions (with a slope of ~1) in Fig. 2.

Incident laser light does not penetrate far into opaque materials such as pyrite, so any near-surface strain will also affect band positions. This effect is not likely to be relevant for growth faces and fracture surfaces,[30] but can cause bands to be upshifted by up to 12 cm$^{-1}$ if samples are prepared mechanically,[14] i.e., by polishing.[14,30,31]

### *Phonon Confinement*

In various nanometer-scale (<25 nm diameter) materials, band positions have been shown to vary with analyte size

**Table 1.** Compilation of positions (vibrational frequencies), and ratios of intensities of the bands in published Raman spectra for pyrite.

| Study | Morphology/texture | $E_g$ mode ($cm^{-1}$) | $A_g$ mode ($cm^{-1}$) | $T_g(3)$ mode ($cm^{-1}$) | $A_g$ intensity/ $E_g$ intensity |
|---|---|---|---|---|---|
| White[1] | Euhedral, macroscopic | 343 | 379 | 430 | 1.02–1.38 |
| | | 344 | 378 | N/A | ~1.2 |
| Vogt et al.[2] | Euhedral, macroscopic | 343 | 379 | 430 | ~3.5 |
| Mernagh and Trudu[3] | Euhedral,macroscopic | 342 | 377 | 428 | ~1.5 |
| Kleppe and Jephcoat[4] | Microcrystal | 344 | 379 | 430 | ~2.2 |
| Danise et al.[5] | Framboidal, polished | 342 | 379 | 432 | ~1.25 |
| Cavalazzi et al.[6] | Framboidal, polished | 343 | 379 | 430 | ~1.25 |
| Borjigin et al.[7] | Framboidal, polished | 343 | 379 | 432 | ~1.6 |
| | | 343 | 379 | 430 | ~1.4 |
| Xu et al.[8] | Microsphere, nanocrystals | 338 | 374 | 424 | ~1 |
| Wei et al.[9] | Nanochain | 335 | 371 | 421 | ~1.6 |
| Mao et al.[10] | Nanocrystal, euhedral | 338 | 371 | N/A | ~2.2 |
| | | 342 | 377 | N/A | ~2.1 |
| RRUFF[a] R050070 | Euhedral, cubic, macroscopic, polished | 343[b] | 379.2[b] | 430[b] | 0.90 |
| RRUFF[a] R050190 | Euhedral, macroscopic, polished | 343.4[b] | 379.9[b] | 433.6[b] | 3.04 |
| RRUFF[a] R070692 | Euhedral, "fine-grained," macroscopic | 340.8[b] | 374[b] | 425[b] | 1.94 |
| Range of values | | 335–344 $\Delta = 9\ cm^{-1}$ | 371–379.9 $\Delta = 8.9\ cm^{-1}$ | 421–433.6 $\Delta = 12.6\ cm^{-1}$ | 0.90–3.5 |

[a]The RRUFF Project is an online database (rruff.info) for Raman spectral data.[12,13] Files of spectral intensity vs. frequency shifts are publicly available and were assessed quantitatively.
[b]When not explicitly listed in published papers, band positions and intensity ratios were determined by the present authors by inspection of enlarged printouts of the spectra.
N/A, not reported; macroscopic, a grain size of >100 μm.

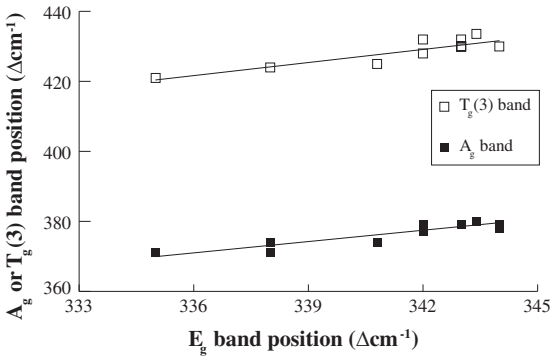


**Figure 2.** The positions of the three dominant bands for pyrite (~343, ~379, and ~430 $\Delta cm^{-1}$), as reported in the literature (Table 1). The positions of the three bands co-vary, with slopes of ~1.

due to a phonon (lattice vibration) confinement effect.[17,32–44] This effect is expected to be relevant for nanometer-scale pyrite, and could result in band downshifts of $>10\ cm^{-1}$ if grains are <5 nm in diameter.[32]

### *Trace Element Chemistry*

The presence of trace elements (TEs) in substitutional solid solution can, due to their differences in atomic mass from that of Fe, shift the positions of the Raman bands for pyrite. For example, Pačevski et al.[31] found that natural pyrite with ~8 wt% Cu (inferred to be in solid solution) yielded Raman spectra with $E_g$, $A_g$, and $T_g(3)$ bands downshifted by ~11 $cm^{-1}$, ~2 $cm^{-1}$, and ~13 $cm^{-1}$, suggesting that band position variation in pyrite due to solid solution is not inherently likely to be uniform for all bands. Additionally, of all TE contents reported, for most natural pyrites only Ni, Co, Se, and As are likely to be present predominantly within the unit cell, while others (Cu, Zn, Pb, Bi, Sb, Tl, Mo, Ag, Cd, Mn, Hg, and Te) can occur both within the unit cell and in micro-inclusions within matrix material or other sulfide minerals.[45]

## Potential Causes of Variability in Band Intensity Ratios

It is well-known that band intensity and area ratios depend on crystal orientation with respect to the polarization plane

of the incident laser beam,[15] as has been demonstrated for other minerals (e.g., phlogopite).[46,47] Accordingly, analyses of faces representing different crystallographic planes through the pyrite unit cell (i.e., {100} versus {111} versus {210})[48] or rotation of a single face on a horizontal stage should result in appreciable changes in band intensity and area ratios.

In summary, for a suite of unpolished, larger than nano-sized pyrite crystals analyzed under the same instrumental and calibration conditions, one might expect differences both in: (1) band positions, due to compositional variations and differential laser heating; and (2) the relative intensities of bands, due to crystal orientation with respect to the plane of polarization of the laser.

## Methods and Materials

In order to test the above hypotheses, three series of experiments were conducted using a fiber optically coupled Raman microprobe (HoloLab Series 5000, Raman Microprobe, Kaiser Optical Systems, Inc.). The spectral region of 100–4000 $\Delta cm^{-1}$ was recorded using an excitation wavelength of 532 nm from a frequency-doubled Nd:YAG laser. Further details on the Raman system's calibration are found in the online Supplemental Material (Raman Instrumental and Methods Specifications, p. 2). The effect of the inherently strong polarization of the laser combined with some depolarization from other optical elements in the beam path produced a transmission ratio in the *x*,*y* directions of 25:2. We used GRAMS/32 AI v.6.00 spectroscopy software (Thermo Scientific) to fit bands (using a combined Gaussian–Lorentzian band shape), and thereby calculate band position, intensity, and area values. The spectral resolution for all spectra herein is 2.5 $cm^{-1}$. For all experiments on pyrite, a 50 $\times$ objective (N.A. = 0.55) was used and analyzed faces were oriented perpendicular to the laser beam. Daily instrumental precision for band positions ($\pm$0.1 $cm^{-1}$) was determined by analysis of a Si wafer (100) at maximum laser power, using the 80 $\times$ objective, at the start and end of each analysis session.

First, to test the effect of laser-induced heating on the band positions as a function of crystal size, we collected spectra (20 spectra of 1 s duration, averaged; these settings were sufficient to produce high ratios of signal-to-noise [S/N]) for three unpolished pyrite samples (Fig. S1) measuring $\sim$1 cm, $\sim$100 $\mu$m, and $\sim$1 $\mu$m in diameter. To change the (unmeasured) temperature at the surface of the crystal, the power density on the sample surface was changed by adjusting the laser power to the sample surface (measured, as in Fig. S2). The laser power was evaluated between spectral collections without moving the sample by collecting a Raman spectrum from a polished silicon wafer mounted adjacent to the sample. The silicon wafer had been calibrated by recording its count rate as a function of the laser power measured by a laser power meter (Metrologic Instruments, Inc.). The silicon was always measured in the same orientation, using an 80 $\times$ ultra-long-working distance Olympus objective (NA = 0.75). The average error of the laser power based on the measured count rate was 0.1 mW.

Second, to evaluate the range in band positions among typical geological samples, we analyzed unpolished faces on five pyrite samples from worldwide localities (Fig. S3) on which we obtained chemical analyses (see below). To avoid excessive sample heating, a laser power of 1 mW at the sample surface was used. For these experiments, 32 spectra of 4 s duration were collected and averaged, as the previously used 20 spectra of 1 s duration did not result in sufficiently high S/N for every sample. The instrumental reproducibility for the positions of the $E_g$, $A_g$, and $T_g(3)$ bands ($1\sigma$ = 0.02, 0.03, and 0.1 $\Delta cm^{-1}$) was determined by collecting ten spectra on the same spot on a single sample, moving away from the spot and defocusing between each spectral collection. For 2 g of the same samples, the abundances of Ni, Co, Se, As, Cu, Zn, Pb, Bi, Tl, Mo, and Te were measured by Activation Laboratories (ON, Canada) using ICP-MS.

Finally, to test the effect of crystal orientation on the intensity and area ratios of bands, centimeter-scale samples (Fig. S4) featuring {100}, {111}, and {210} faces,[48] were mounted on a rotating stage and rotated clockwise, with 20 spectra of 1 s duration collected and averaged at 10° increments. This experiment was repeated using two different laser powers: 5 mW, and the highest achievable, 14.4 mW. Although the reproducibility of the intensity and area ratios of the $A_g$ and $E_g$ bands was measured to be $\pm$0.01 ($1\sigma$) at 1 mW, 5 mW, and 14.4 mW, the 5 mW and 14.4 mW laser powers offered improved S/N, and peaks were fit with higher confidence ($R^2 > 0.997$). Due to the high laser powers used in this test, sample heating likely modified the resultant data, though any modifications were modulated by the use of large ($\sim$1 cm) pyrite crystals.

Data from all reproducibility tests are listed in the Supplemental Material, Table S1.

## Results

### *Effects of Sample Heating on Spectra*

As laser power was increased, all bands were downshifted (Fig. 3; Fig. S5) and, in general, broadened (Fig. S6). The downshifting of bands with respect to laser power was approximately linear in most cases (Fig. 3). The magnitude of this effect and the lowest wavenumber positions attained by each band were also negatively correlated with the grain size of the analyte (Fig. 3; Table 2). The total downshifting was greatest for the $A_g$ band, followed by the $T_g(3)$ band, and then the $E_g$ band (Fig. 3; Table 2). The lowest wavenumber positions (in Table 2) were constrained by: (1) the

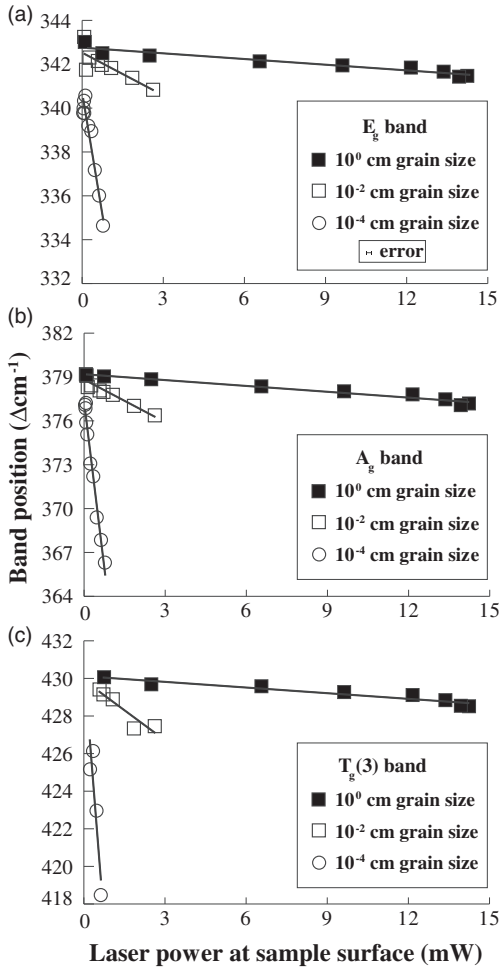


**Figure 3.** Changes in the position of the (a) $E_g$, (b) $A_g$, and (c) $T_g(3)$ bands, with an increase in laser power at the sample surface. The average laser power measurement error was $\pm 0.1$ mW. Instrumental reproducibility ($1\sigma$) for band positions varied with laser power and between bands (Table S1) but was always smaller than the symbols used here, so is not shown.

**Table 2.** The lowest wavenumber positions attained by each Raman band in the laser heating experiment, using the 50 × objective, for analytes with different grain sizes.

| Grain diameter (cm) | Lowest wavenumber band position ($cm^{-1}$) | | |
|---|---|---|---|
| | $E_g$ | $A_g$ | $T_g(3)$ |
| 1 | 341.4 ($\Delta = 0.6$) | 377.1 ($\Delta = 1.9$) | 428.5 ($\Delta^a = 1.5$) |
| 0.01 | 340.8 ($\Delta = 1.2$) | 376.4 ($\Delta = 2.6$) | 427.3 ($\Delta = 2.7$) |
| 0.001 | 334.6 ($\Delta = 7.4$) | 366.3 ($\Delta = 12.7$) | 418.5 ($\Delta = 11.5$) |

[a]Here, $\Delta$ refers to the downshift of each band from the "ideal" position, taken as 342, 379, and 430 $\Delta cm^{-1}$, for the E, $A_g$ and $T_g(3)$ bands, respectively.[1]

maximum attainable laser power at the sample's surface for the analytical setup (14.4 mW); and (2) the maximum laser power reached without apparent volatilization of the sample ($\sim 2.6 \pm 0.1$ mW for the 0.01 cm-diameter fragment; $\sim 0.8 \pm 0.1$ mW for the 1 μm-diameter framboidal microcrystal; no volatilization was apparent for the 1 cm-diameter crystal), which was indicated both by lack of visible alteration of the sample and absence of newly created Raman bands (e.g., at ~217 and 282.4 $\Delta cm^{-1}$). It also should be noted on Fig. 3 that even at the lowest laser powers employed (~0.1 mW), greater downshifts in peak position occurred in the smaller, compared to the larger grains.

### *Spectral Differences Among Samples*

The five geologic samples measured under constant analytical conditions yielded spectra with slightly different positions for the same bands (Table 3, Fig. 4). The positions of the $A_g$ and $T_g(3)$ bands co-vary with those of the $E_g$ band, but with different slopes (Fig. 4a and 4b) to those for bands in published spectra (Fig. 2). Other spectral parameters such as band area and intensity ratios are explored in the Supplemental Material (Fig. S7).

The samples additionally exhibit variable TE content (Table 3; Table S2). In the context of the present study, the most important message is that the wavenumber range among these "typical" pyrite samples (Table 3) is only about one-tenth of that shown in Raman spectra in the pyrite literature (Table 1, Fig. 2).

## Spectral Differences Due to Crystallographic Orientation Within a Sample

### *{100} Faces, Cubic Pyrite*

At a laser power of 5 mW, the average intensity ratio of the $A_g$ band relative to the intensity of the $E_g$ band was $0.99 \pm 0.05$ ($2\sigma$) (Fig. 5a). The intensity ratio varied slightly as the sample was rotated from 0° (in which a pair of vertical faces were oriented parallel to the laser's plane of polarization) to 360°, and peaked when the face was oriented at 0° (or 360°), 90°, 180°, and 270°, with minima at 45°, 135°, 225°, and 315°. The average area ratio of the $A_g$ band relative to the area of the $E_g$ band was $0.97 \pm 0.06$ ($2\sigma$) (Fig. 5a). The area ratio also peaked at 0°, 90°, 180°, and 270°, with minima at 45°, 135°, 225°, and 315°. Note that the maxima at 90° and 270° were of slightly greater amplitude than those at 0° and 180°. Likewise, the minima at 45° and 225° were of slightly greater amplitude than those at 135° and 315°.

The full width half-maximum (FWHM) values of the $E_g$ and $A_g$ bands were generally smallest when the band area ratios peaked, at 0°, 90°, 180°, and 270°

**Table 3.** Summary of Raman band positions and TE abundances for the geologic samples used in this experiment. Sample names correspond to labels in Fig. S3.

| Sample | $E_g$ band position ($\Delta cm^{-1}$) | $A_g$ band position ($\Delta cm^{-1}$) | $T_g(3)$ band position ($\Delta cm^{-1}$) | Ni (wt%) | Co (wt%) | Se (wt%) | As (wt%) |
|---|---|---|---|---|---|---|---|
| A | 342.9 | 379.2 | 430.5 | 0.0006 | 0.0001 | <0.0001 | 0.0491 |
| B | 342.8 | 379.2 | 430.5 | 0.0002 | <0.0001 | 0.0009 | 0.0279 |
| C | 342.9 | 379.3 | 430.4 | 0.1174 | 0.0112 | <0.0001 | 0.0033 |
| D | 342.6 | 379.0 | 430.0 | 0.0002 | 0.0004 | 0.0013 | 0.9875 |
| E | 342.1 | 378.0 | 429.8 | 0.0028 | 0.0091 | 0.0019 | 0.0399 |
| Range of values | 342.1–342.9 | 378.0–379.2 | 429.8–430.5 | 0.0002–0.1174 | <0.0001–0.0112 | <0.0001–0.0019 | 0.0033–0.9875 |

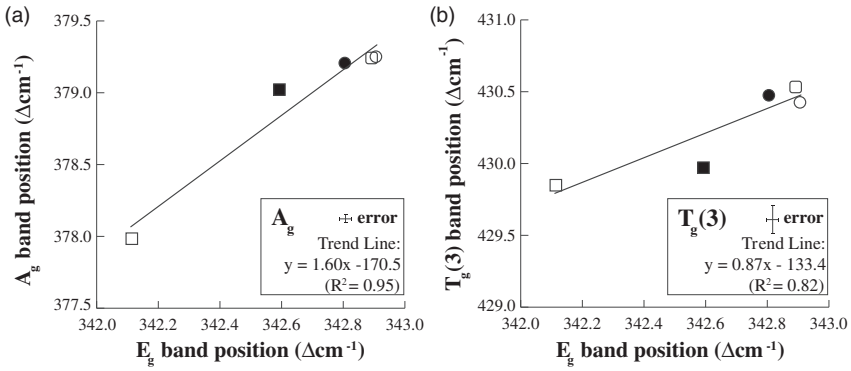


**Figure 4.** The positions of bands generated from five macroscopic pyrite samples (see Fig. S3) from different localities. (a) $A_g$ plotted vs. $E_g$, (b) $T_g(3)$ plotted vs. $E_g$. The different symbols correspond to different samples in Table 3: open rounded square = A; filled circle = B; open circle = C; filled square = D, and open square = E. Error bars in legend correspond to 1σ instrumental reproducibility data (Table S1).

(FWHM ~4.4–4.7 $cm^{-1}$, compared with typical values of ~4.8–5.1 $cm^{-1}$; Fig. S8). The very small (~0.2 $cm^{-1}$) variations in the band positions showed no obvious trend with sample rotation.

At a laser power of 14.4 mW, the average intensity ratio of the $A_g$ band relative to the intensity of the $E_g$ band was $0.76 \pm 0.54$ (2σ) (Fig. 5b). The average area ratio of the $A_g$ band relative to the area of the $E_g$ band was $1.1 \pm 0.13$ (2σ) (Fig. 5b). Intensity ratio variations during rotation were much larger, but less clearly defined, at 14.4 mW compared to 5 mW. As the FWHM of the $A_g$ band increased during rotation, the intensity ratio of the $A_g$ and $E_g$ bands decreased as a negative power function (Fig. S9), and the $A_g$ band was downshifted (Fig. S10).

## {111} Faces, Octahedral Pyrite

In the starting orientation (0°) of the crystal, one exterior edge of the (111) face was perpendicular to the laser's plane of polarization. At a laser power of 5 mW, the average intensity ratio of the $A_g$ band relative to $E_g$ band was $1.84 \pm 0.08$ (2σ) (Fig. 6a). The average area ratio of the $A_g$ band relative to the $E_g$ band was $1.77 \pm 0.06$ (2σ). Although the data acquired at 5 mW in Fig. 6a show small-amplitude oscillations, there is no clear relationship between angle of rotation and the ratios of band intensities or areas. There is no correlation between any band's FWHM value and: (1) its position; (2) its intensity ratio; or (3) its area ratio.

At a laser power of 14.4 mW, the average intensity ratio of the $A_g$ band relative to the $E_g$ band was $1.93 \pm 0.06$ (2σ) (Fig. 6b). The average area ratio of the $A_g$ band relative to the $E_g$ band was $2.08 \pm 0.1$ (2σ). As at 5 mW, there is no correlation between any band's FWHM value and: (1) its position; (2) its intensity ratio; or (3) its area ratio.

## {210} Faces, Pyritohedral Pyrite

In the chosen starting orientation of the crystal, the longest edge of the (210) face was oriented perpendicularly to the laser's plane of polarization. At a laser power of 5 mW, the average intensity ratio of the $A_g$ band relative to the $E_g$ band

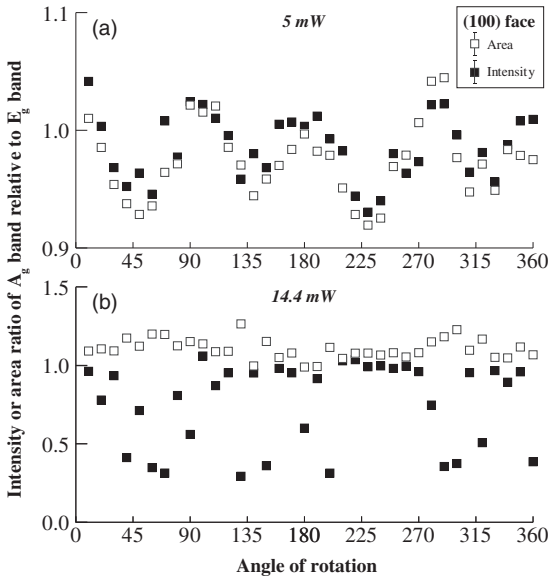


**Figure 5.** Changes in the intensity and area ratios of the $A_g$ band relative to the $E_g$ band, with rotation of a (100) face, at laser powers of (a) 5 mW and (b) 14.4 mW. Error bars in legend correspond to 1σ instrumental reproducibility data (Table S1) for (a), but error bars for (b) are smaller than the symbols used, so are not shown.

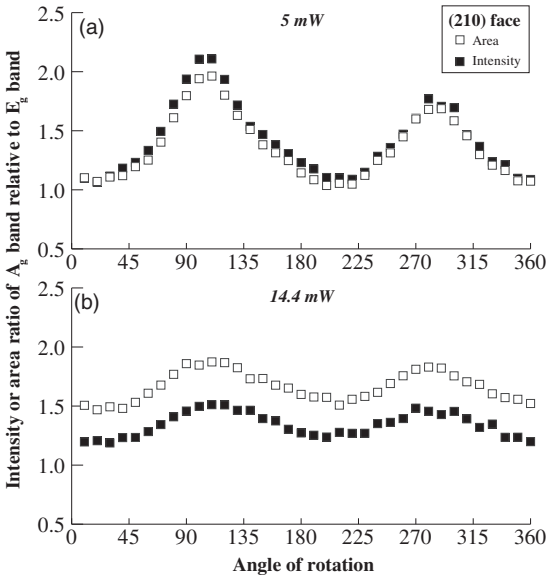


**Figure 7.** Changes in the intensity and area ratios of the $A_g$ band relative to the $E_g$ band, with rotation of a (210) face, at laser powers of (a) 5 mW and (b) 14.4 mW. Instrumental reproducibility (1σ) (Table S1) was smaller than the symbols used here, so is not shown.

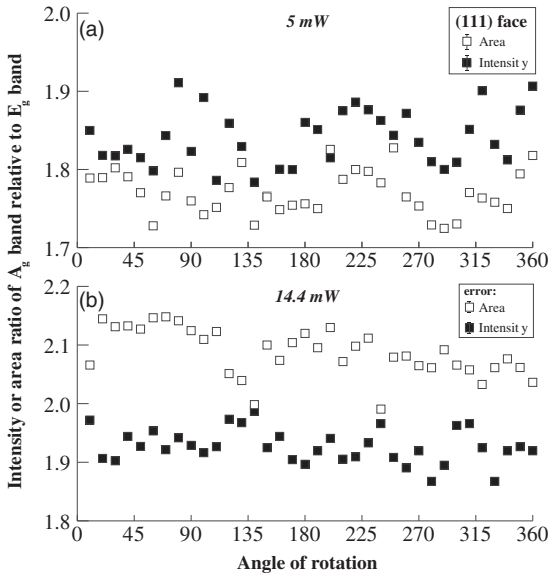


**Figure 6.** Changes in the intensity and area ratios of the $A_g$ band relative to the $E_g$ band, with rotation of a (111) face, at laser powers of (a) 5 mW and (b) 14.4 mW. Error bars in legends of (a) and (b) correspond to 1σ instrumental reproducibility data (Table S1).

was 1.41 ± 0.6 (2σ) (Fig. 7a). The average area ratio of the $A_g$ band relative to the $E_g$ band was 1.35 ± 0.54 (2σ). The origin of the large standard deviations is a clear 180° periodicity in both datasets, with minima at ~20° and 200° and maxima at ~110° and ~290° (the exact rotational positions being a function of the "arbitrary" starting orientation). The second maximum has smaller amplitude than the first. Periodicity of a different type occurs in the FWHM (Fig. S11a) and band position (Fig. S12) data with rotation. For each of them, a single broad maximum occurs at ~200° and a much narrower local maximum occurs at ~290–310°.

At a laser power of 14.4 mW, the average intensity ratio of the $A_g$ band relative the $E_g$ band was 1.34 ± 0.21 (2σ) (Fig. 7b). The average area ratio of the $A_g$ band relative to the $E_g$ band was 1.66 ± 0.25 (2σ). Again, the origin of the large standard deviations is a 180° periodicity in both data sets, with minima at ~10–20° and ~190–210°, and maxima at ~110° and ~280–290° (Fig. 7b). In contrast to the 5 mW experiment, there is no apparent periodicity in the FWHM (Fig. S11b) or band position data (Fig. S12). The FWHM and band position data are discussed further in the Supplemental Material (p. 15).

## Discussion

Our observation that increasing laser power leads to downshifted (Fig. 3; Fig. S5) and broadened (Fig. S6) Raman bands, particularly for small grains (Fig. 3), strongly supports the hypothesis that there exists a temperature effect for the Raman spectrum of pyrite. The observed volatilization or oxidation of the 0.01 cm- and 1 μm-diameter samples at laser powers of 2.6 ± 0.1 mW and 0.8 ± 0.1 mW, respectively, provides further evidence that

the observed changes in the Raman spectrum were in direct response to rising temperature at the sample surface. The major difference between these two observed types of heating effects is that the former represents a nondestructive, reversible displacement of atoms and the latter, the destruction of the mineral. It is also worth noting that the literature band positions farthest from the typical values are for nanocrystals (Table I)—an observation of the variation in band positions with grain size, which this study explains.

When laser power and objective N.A. were held constant, Raman spectra for pyrite samples of various morphologies and provenance demonstrated a narrow range in the positions of each of the three bands (Fig. 4; Table 3), about one-tenth of the range we have found to be attributable to laser heating (Fig. 3; Table 2). The strong positive correlations ($R^2 > 0.94$) between the relative areas and relative intensities of the bands (Fig. S7) rule out differential heating as the cause of this (small) intersample variability because heating results in band-broadening in spectra (Fig. S6), thereby weakening the correlation between relative intensities and relative areas of bands. We thus suggest that the variations in band positions among these samples likely are related to physical–chemical differences among them, such as in TE content (Table 3; Table S2). Importantly, these TE differences are associated with no more than a $0.8 \pm 0.04$, $1.3 \pm 0.06$, and $0.7 \pm 0.2\,cm^{-1}$ difference for positions of the $E_g$, $A_g$, and $T_g(3)$ bands.

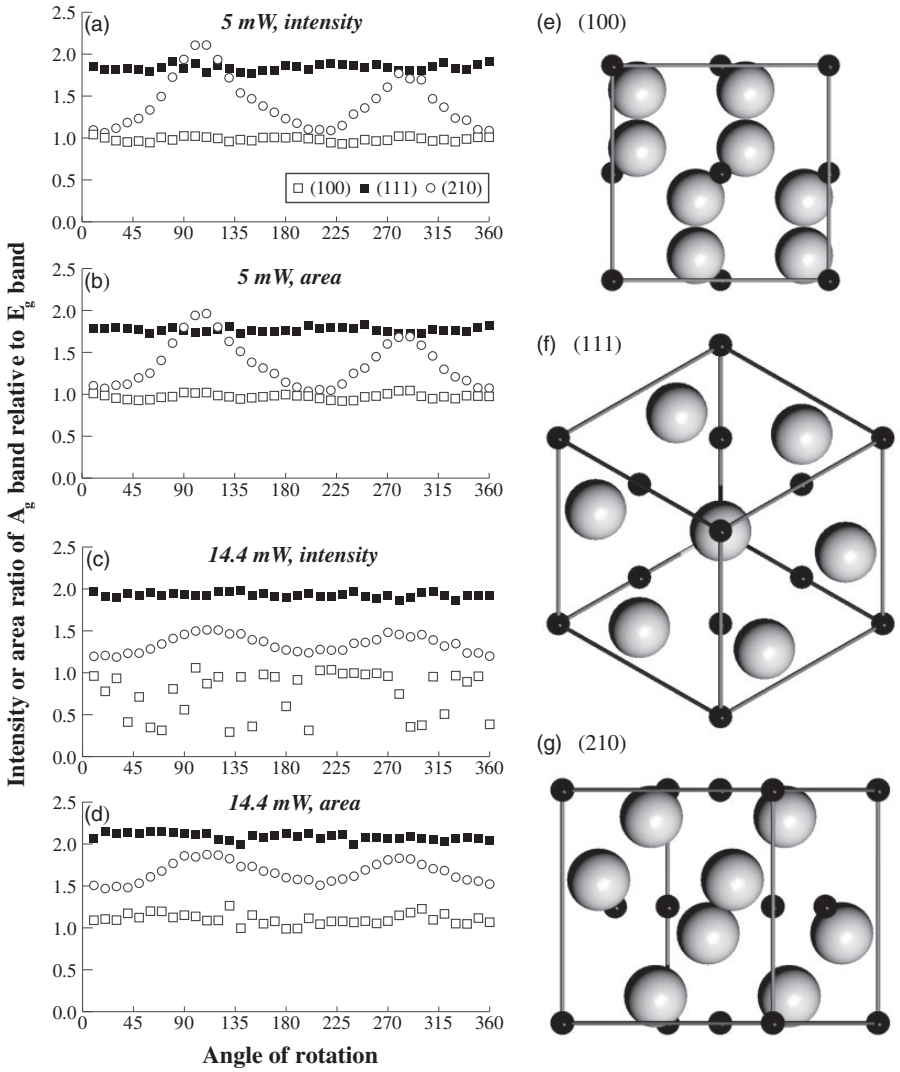


**Figure 8.** Changes in the intensity (a and c) and area (b and d) of the $A_g$ band relative to the $E_g$ band, with rotation of (100), (111), and (210) pyrite faces (distinguished by symbols), at laser powers of 5 mW (a, b), and 14.4 mW (c, d). Instrumental reproducibility ($1\sigma$) (Table S1) was smaller than the symbols used here, so is not shown. The unit cell of pyrite,[49] visualized in XtalDraw,[50] looking perpendicularly onto (e) the (100) face, (f) the (111) face, and (g) the (210) face. Gray spheres represent $S^{2-}$, black spheres $Fe^{2+}$. Only one S–S dumbbell is visible, at the center of the unit cell. The remaining S atoms are bonded to S atoms in adjacent unit cells.

The observed covariance of area and intensity ratios (Figs. 5a, 6a, 6b, 7a, and 7b) with rotation of (100), (111), and (210) faces suggests that, rather than being subject to a differential rotation-dependent broadening of the $A_g$ and $E_g$ bands, both ratios are a function of the relative degrees of excitation of the $A_g$ mode compared to the $E_g$ mode for pyrite, which depend on the crystallographic orientation with respect to the plane of polarization of the incident laser beam. The clear oscillations of the (100) and (210) data with rotation are likely a function of the two-fold symmetry of crystal structure of pyrite as viewed perpendicularly to the (100) and (210) faces (Fig. 8e and 8g). The lack of covariation of area and intensity ratios with rotation of the (100) face at a laser power of 14.4 mW (Fig. 5b) can likely be attributed to greater thermal broadening of the $A_g$ band relative to the $E_g$ band at random angles of rotation (Figs. S8b, S9, and S10 as discussed further in the Supplemental Material, p. 12). Differences in the average ratios of band areas and intensities between the crystallographic planes analyzed here, and changes in ratios of band areas and intensities with rotation of these individual crystallographic planes (summarized in Fig. 8), are likely the result of directionally dependent differential excitation of the $E_g$ and $A_g$ modes.

For geologic applications, the most important finding is that, despite their spectral variations due to rotation, the different face types (i.e., crystallographic planes) of pyrite still can be clearly distinguished by the values of their typical band intensity ratios. Particularly at a laser power of 14.4 mW, the average ($\pm 2\sigma$) band intensity ratios and area ratios for the three crystallographically different face types do not overlap (Fig. 8c and 8d). Based on this relationship, Raman microprobe analysis in which the laser beam is approximately perpendicular to the mineral face could be used to distinguish among these three face types on pyrite samples, regardless of rotation. The specific laser power needed will depend on the instrument configuration and the degree of heat dissipation for the pyrite samples under consideration. Given that certain face types represent specific pyrite morphologies (e.g., the {210} form represents the pyritohedral morphology), Raman microprobe analysis could be used to infer crystal morphology, although connection of samples to a good heat-sink may be necessary to prevent volatilization of nano-/microcrystalline pyrites.

## Conclusion

We have determined the magnitude of several effects on the Raman spectrum of pyrite. First, the heating effect identified here can cause sufficient downshift in Raman bands to encompass and also explain most of the band position variability in previously reported Raman spectra for pyrite. The magnitude of this effect, which is far greater than that likely to result from differential calibration, can be reduced through the use of lower laser powers, by analyzing larger grains, or by ensuring that the analyte is connected to a good heat-sink. If laser heating is demonstrably avoided, Raman band positions may be related to physical–chemical differences (e.g., TE content) among samples. However, it is worth noting that several of the literature data are from polished samples (a common state for geologic samples being studied). Further work is necessary to extend the results of the present study to polished sections, which would include evaluation of the effects of different polishing techniques.

Second, we confirmed the expectation that the band intensity ratios in Raman spectra for pyrite vary due to changes in unit cell orientation with respect to the plane of polarization of the laser. Given that the band intensity ratios were distinguishable for the three most commonly developed face types on pyrite, laser Raman microprobe analysis could be used to infer pyrite crystal morphology in sedimentary records, even when pyrite is present in trace amounts and of very fine grain size. Future work will involve developing a method applicable to framboidal pyrites, then experimentally calibrating the relationship between various environmental conditions and pyrite crystal morphology. Because different morphologies are thought to reflect different formation conditions (e.g., degrees of supersaturation),[51] Raman-based determination of the crystal morphology of naturally occurring pyrite could then potentially be used as a method for inferring specific environmental conditions at the location of pyrite formation.

This work should serve as a blueprint for those wishing to use laser Raman microprobe analysis to characterize pyrite and, perhaps, other unpolished opaque phases after testing as documented here. It is clear that the experimental set-up (laser wavelength and power, objective NA) and physical nature of the sample (grain size, morphology, and orientation) are of paramount importance in determining the position, relative intensity, and relative area of Raman bands. A Raman spectrum is thus of limited diagnostic use without accompanying information on the experimental setup and samples analyzed. To promote inter-laboratory consistency, published Raman spectral studies should also report detailed information on their instrument calibration procedure.

### Acknowledgments

The authors thank four anonymous reviewers and the editor, whose comments greatly improved the manuscript. They especially thank Dr. John Freeman for his helpful comments on an earlier version of the manuscript. Additionally, they thank the members of the Fike and Bradley Labs at Washington University, whose enthusiastic discussions yielded several useful additions and improvements to this work. RNB gratefully acknowledges support from the McDonnell Center for the Space Sciences at Washington University in St. Louis.

## Conflict of Interest

The authors report there are no conflicts of interest.

## Funding

Funding for this work was generously provided by the Packard Foundation and McDonnell Center for the Space Sciences.

## Supplemental Material

All supplemental material mentioned in the text, including 12 figures, two tables, and additional discussion thereof, is available in the online version of the journal.

## References

1. S.N. White. "Laser Raman Spectroscopy as a Technique for Identification of Seafloor Hydrothermal and Cold Seep Minerals". Chem. Geol. 2009. 259(3): 240–252.
2. H. Vogt, T. Chattopadhyay, H.J. Stolz. "Complete First-Order Raman Spectra of the Pyrite Structure Compounds FeS2, MnS2 and SiP2". J. Phys. Chem. Solids. 1983. 44(9): 869–873.
3. T.P. Mernagh, A.G. Trudu. "A Laser Raman Microprobe Study of Some Geologically Important Sulfide Minerals". Chem. Geol. 1993. 103(1): 113–127.
4. A. Kleppe, A. Jephcoat. "High-Pressure Raman Spectroscopic Studies of $FeS_2$ Pyrite". Mineral. Mag. 2004. 68(3): 433–441.
5. S. Danise, B. Cavalazzi, S. Dominici, F. Westall, et al. "Evidence of Microbial Activity from a Shallow Water Whale Fall (Voghera, Northern Italy)". Palaeogeogr. Palaeoclimatol. Palaeoecol. 2012. 317–318: 13–26.
6. B. Cavalazzi, R. Barbieri, S.L. Cady, A.D. George, et al. "Iron-Framboids in the Hydrocarbon-Related Middle Devonian Hollard Mound of the Anti-Atlas Mountain Range in Morocco: Evidence of Potential Microbial Biosignatures". Sediment. Geol. 2012. 263–264: 183–193.
7. T. Borjigin, L. Yin, L. Bian, X. Yuan, et al. "Nano-Scale Spheroids and Fossils from the Ediacaran Doushantuo Formation in China". Open Paleo. J. 2014. 5: 1–9.
8. J. Xu, H. Xue, X. Yang, H. Wei, et al. "Synthesis of Honeycomb-Like Mesoporous Pyrite FeS2 Microspheres as Efficient Counter Electrode in Quantum Dots Sensitized Solar Cells". Small. 2014. 10(22): 4754–4759.
9. Z.H. Wei, Y.C. Qiu, H.N. Chen, K.Y. Yan, et al. "Magnetic-Field-Assisted Aerosol Pyrolysis Synthesis of Iron Pyrite Sponge-Like Nanochain Networks as Cost-Efficient Counter Electrodes in Dye-Sensitized Solar Cells". J. Mater. Chem. A. 2014. 2(15): 5508–5515.
10. B. Mao, Q. Dong, C.L. Exstrom, J. Huang. "Surface Thermal Stability of Iron Pyrite Nanocrystals: Role of Capping Ligands". Thin Solid Films. 2014. 562: 361–366.
11. C. Sourisseau, R. Cavagnat, M. Fouassier. The Vibrational Properties and Valence Force Fields of FeS2, RuS2 Pyrites and FeS2 Marcasite". J. Phys. Chem. Solids. 1991. 52(3): 537–544.
12. R.T. Downs. "The RRUFF Project: An Integrated Study of the Chemistry, Crystallography, Raman and Infrared Spectroscopy of Minerals". In: Program and Abstracts of the 19th General Meeting of the International Mineralogical Association. Kobe, Japan: July 23, 2006. Pp. 13.
13. B. Lafuente, R.T. Downs, H. Yang, N. Stone. "The Power of Databases: The RRUFF Project". In: T. Armbruster, R.M. Danisi, editors. Highlights in Mineralogical Crystallography. Berlin, Germany: W. De Gruyter, 2015. Pp. 1–30.
14. L. Nasdala, O. Beyssac, W.J. Schopf, B. Bleisteiner. "Application of Raman-Based Images in the Earth Sciences". In: A. Zoubir, editor. Raman Imaging – Techniques and Applications. Springer Series in Optical Sciences. Berlin, Heidelberg, Germany: Springer, 2012. Vol. 168, Pp. 145–187.
15. L. Nasdala, D.C. Smith, R. Kaindl, M.A. Ziemann. "Raman Spectroscopy: Analytical Perspectives in Mineralogical Research". In: A. Beran, E. Libowitzky, editors. Spectroscopic Methods in Mineralogy. EMU Notes in Mineralogy Series. Budapest, Hungary: Eötvös University Press, 2004. Vol. 6, chap. 7, Pp. 281–343.
16. N.J. Everall, J. Lumsdon, D.J. Christopher. "The Effect of Laser-Induced Heating upon the Vibrational Raman Spectra of Graphites and Carbon Fibres". Carbon. 1991. 29(2): 133–137.
17. G. Viera, S. Huet, L. Boufendi, E. Bertran. "Crystal Size and Temperature Measurements in Nanostructured Silicon Using Raman Spectroscopy". J. Appl. Phys. 2001. 90(8): 4175–4183.
18. F. Huang, K. Yue, P. Tan, S.L. Zhang, et al. "Temperature Dependence of the Raman Spectra of Carbon Nanotubes". J. Appl. Phys. 1998. 84(7): 4022–4024.
19. H.D. Li, K.T. Yue, Z.L. Lian, Y. Zhan, et al. "Temperature Dependence of the Raman Spectra of Single-Wall Carbon Nanotubes". Appl. Phys. Lett. 2000. 76: 2053–2055.
20. N. Raravikar, P. Keblinski, A. Rao, M. Dresselhaus, et al. "Temperature Dependence of Radial Breathing Mode Raman Frequency of Single-Walled Carbon Nanotubes". Phys. Rev. B. 2002. 66(23): 1–9.
21. L. Ci, Z. Zhou, L. Song, X. Yan, et al. "Temperature Dependence of Resonant Raman Scattering in Double-Wall Carbon Nanotubes". Appl. Phys. Lett. 2003. 82(18): 3098–3100.
22. A. Bassil, P. Puech, L. Tubery, W. Bacsa, et al. "Controlled Laser Heating of Carbon Nanotubes". Appl. Phys. Lett. 2006. 88(17): 173113.
23. I. Calizo, A.A. Balandin, W. Bao, F. Miao, et al. "Temperature Dependence of the Raman Spectra of Graphene and Graphene Multilayers". Nano. Lett. 2007. 7(9): 2645–2649.
24. P.H. Tan, Y.M. Deng, Q. Zhao, W.C. Cheng. "The Intrinsic Temperature Effect of the Raman Spectra of Graphite". Appl. Phys. Lett. 1999. 74(13): 1818–1820.
25. E. Zouboulis, M. Grimsditch. "Raman Scattering in Diamond up to 1900K". Phys. Rev. B. 1991. 43(15): 3–6.
26. T. Hart, R. Aggarwal, B. Lax. "Temperature Dependence of Raman Scattering in Silicon". Phys. Rev. B. 1970. 1(2): 638–642.
27. R. Tsu, J.G. Hernandez. "Temperature Dependence of Silicon Raman Lines". Appl. Phys. Lett. 1982. 41(11): 1016–1018.
28. C.H. Chio, S.K. Sharma, P.G. Lucey, D.W. Muenow. "Effects of Particle Size and Laser-Induced Heating on the Raman Spectra of Alpha Quartz Grains". Appl. Spectrosc. 2003. 57(7): 774–783.
29. K.P. Bhandari, P.J. Roland, T. Kinner, Y. Cao, et al. "Analysis and Characterization of Iron Pyrite Nanocrystals and Nanocrystalline Thin Films Derived from Bromide Anion Synthesis". J. Mater. Chem. A. 2015. 3(13): 6853–6861.
30. E. Libowitzky. "Anisotropic Pyrite: A Polishing Effect". Phys. Chem. Miner. 1994. 21(1): 97–103.
31. A. Pačevski, E. Libowitzky, P. Živković, R. Dimitrijević, et al. "Copper-Bearing Pyrite From the Čoka Marin Polymetallic Deposit, Serbia: Mineral Inclusions or True Solid-Solution?" Can. Mineral. 2009. 46(1): 249–261.
32. R.P. Wang, G.W. Zhou, Y.L. Liu, S.H. Pan, et al. "Raman Spectral Study of Silicon Nanowires: High-Order Scattering and Phonon Confinement Effects". Phys. Rev. B. 2000. 61(24): 16827–16832.
33. R.J. Nemanich, S.A. Solin, R.M. Martin. "Light Scattering Study of Boron Nitride Microcrystals". Phys. Rev. B. 1981. 23(12): 6348–6356.
34. H. Richter, Z.P. Wang. "The One Phonon Raman Spectrum in Microcrystalline Silicon". Solid State Commun. 1981. 21(3): 625–629.
35. D. Yu, X. Sun, C. Lee, I. Bello, et al. "Synthesis of Boron Nitride Nanotubes by means of Excimer Laser Ablation at High Temperature". Appl. Phys. Lett. 1998. 72: 1966–1968.
36. A.G. Rolo, L.G. Vieira, M.J.M. Gomes, J.L. Ribeiro, et al. "Growth and Characterisation of Cadmium Sulphide Nanocrystals Embedded in Silicon Dioxide Films". Thin Solid Films. 1998. 312(1): 348–353.

37. M.I. Vasilevskiy, A.G. Rolo, M.J.M. Gomes, O.V. Vikhrova, et al. "Impact of Disorder on Optical Phonons Confined in CdS Nano-Crystallites Embedded in a SiO2 Matrix". J. Phys.: Condens. Matter. 2001. 13(14): 3491–3509.
38. R.R. Prabhu, M.A. Khadar. "Study of Optical Phonon Modes of CdS Nanoparticles using Raman Spectroscopy". Bull. Mater. Sci. 2008. 31(3): 511–515.
39. M. Rajalakshmi, A.K. Arora. "Optical Properties of Selenium Nanoparticles Dispersed in Polymer". Solid State Commun. 1999. 110(2): 75–80.
40. M. Rajalakshmi, A.K. Arora, B.S. Bendre, S. Mahamuni. "Optical Phonon Confinement in Zinc Oxide Nanoparticles". J. Appl. Phys. 2000. 87(5): 2445–2448.
41. S. Dash, A. Singh, P.K. Ajikumar, H. Subramanian, et al. "Synthesis and Characterization of Nanocrystalline Thoria Obtained from Thermally Decomposed Thorium Carbonate". J. Nucl. Mater. 2002. 303(2): 156–168.
42. M. Rajalakshmi, A.K. Arora, S. Dash, A.K. Tyagi. "Raman Scattering Investigations of Nanocrystalline Thorium Oxide". J. Nanosci. Nanotechnol. 2003. 3(5): 420–422.
43. K.R. Zhu, M.S. Zhang, Q. Chen, Z. Yin. "Size and Phonon-Confinement Effects on Low-Frequency Raman Mode of Anatase TiO2 Nanocrystal". Phys. Lett. A. 2005. 340(1): 220–227.
44. S. Osswald, V.N. Mochalin, M. Havel, G. Yushin, et al. "Phonon Confinement Effects in the Raman Spectrum of Nanodiamond". Phys. Rev. B: Condens. Matter. 2009. 80(7): 075419(9).
45. R.R. Large, J.A. Halpin, L.V. Danyushevsky, V.V. Maslennikov, et al. "Trace Element Content of Sedimentary Pyrite as a New Proxy for Deep-Time Ocean-Atmosphere Evolution". Earth Planet. Sci. Lett. 2014. 389: 209–220.
46. E. Loh. "Optical Vibrations in Sheet Silicates". J. Phys. C: Solid State Phys. 1973. 6(6): 1091–1104.
47. A. Tlili, D. Smith, J. Beny. "A Raman Microprobe Study of Natural Micas". Mineral. Mag1989. 53, Part 2(370): 165–179).
48. I. Sunagawa. "Variations in Crystal Habit of Pyrite". Report, Geological Survey of Japan, Japan, 1957.
49. P. Bayliss. "Crystal Structure Refinement of a Weakly Anisotropic Pyrite". Am. Mineral. 1977. 62(1945): 1168–1172.
50. R.T. Downs, M. Hall-Wallace. "The American Mineralogist Crystal Structure Database". Am. Mineral. 2003. 88: 247–250.
51. J.B. Murowchick, H.L. Barnes. "Effects of Temperature and Degree of Supersaturation on Pyrite Morphology". Am. Mineral. 1987. 72(11–12): 1241–1250.